

## Ordering tendencies in octahedral MgO-ZnO alloys

Mahdi Sanati,<sup>1</sup> Gus L. W. Hart,<sup>2</sup> and Alex Zunger<sup>1</sup>

<sup>1</sup>National Renewable Energy Laboratory, Golden, Colorado 80401, USA

<sup>2</sup>Department of Physics & Astronomy, Northern Arizona University, Flagstaff, Arizona 86011-6010, USA

(Received 18 August 2003; published 24 October 2003)

Isostructural II-VI alloys whose components are either rocksalt stable (e.g., CaO-MgO) or zincblende stable (e.g., ZnS-ZnSe) are known to be thermodynamically unstable at low temperatures, showing a miscibility gap and no bulk ordering. In contrast, we show that *heterostructural* MgO-ZnO is stable, under certain conditions, in the sixfold-coordinated structure for Zn concentrations below 67%, giving rise to spontaneously ordered alloys. Using first-principles calculations, we explain the origin of this stability, the structures of their low-temperature ordered phases, short-range-order patterns, and their optical band-gap properties.

DOI: 10.1103/PhysRevB.68.155210

PACS number(s): 71.55.Gs, 71.20.Nr

### I. INTRODUCTION

Binary II-VI compounds appear<sup>1</sup> largely as fourfold-coordinated (CN4) zincblende/wurtzite structures (ZnO, ZnS, ZnSe, ZnTe, CdS, CdSe, and CdTe) or as sixfold-coordinated (CN6) rocksalt structures (MgO, CaO, and CdO). Isovalent and isostructural alloys of II-VI constituents are generally thermodynamically unstable, in that their mixing enthalpy, in either the CN6 rocksalt (*B1*) structure or in the CN4 (*B3*) or wurtzite (*B4*) structures,

$$\Delta H_{\alpha}(A_xB_{1-x}C) = E_{\alpha}(A_xB_{1-x}C) - [xE_{\alpha}(AC) + (1-x)E_{\alpha}(BC)], \quad (1)$$

is *positive*.<sup>2-4</sup> Here,  $\alpha$  denotes fourfold or sixfold coordinated crystal structure, and  $E_{\alpha}(AC)$  is the total energy of compound  $AC$  in crystal structure  $\alpha$ . For example,  $\Delta H_{B1}$  of isovalent alloys whose constituents are *B1* stable (CaO, MgO, and CdO) are generally positive,<sup>2</sup> as are  $\Delta H_{B3}$  of isovalent alloys<sup>4</sup> whose constituents are *B3* stable (ZnS, ZnSe, and ZnTe). This can be seen both experimentally<sup>2,3</sup> and from local-density approximation (LDA) total-energy calculations on 50–50% alloys, modeled via (quasirandom) supercells.<sup>4</sup> Because  $\Delta H > 0$ , the isovalent and isostructural alloys can be thermodynamically miscible only at high temperatures where the entropy term  $-TS$  is sufficiently negative. However, as the temperature is lowered, the alloys phase separate, showing no ordered intermediate structures.<sup>3</sup>

An interesting case is an *isovalent* II-VI alloy made from *nonisostructural* components, e.g., wurtzite+rocksalt (*B4-B1*). Such alloys, e.g., ZnO-MgO became of great interest recently,<sup>5</sup> since in principle a *B4-B1* combination spans a wider range of optical band gaps than either a *B1-B1* or a *B4-B4* alloy. For example, alloys of ZnO ( $E_g = 3.4$  eV) with MgO ( $E_g = 7.7$  eV) could span a range from blue to deep UV, which is of interest for optical laser and light-emitting diode applications.<sup>5</sup> However, it is not known if nonisostructural II-VI alloys are, in principle, thermodynamically stable or not.

### II. SUMMARY OF FINDINGS

We report here on first-principles total-energy calculations which show the following.

(1) Sixfold-coordinated  $Mg_{1-x}Zn_xO$  alloys have  $\Delta H_{B1} < 0$  for Mg-rich compositions, in contrast with the opposite sign for isostructural *B1* oxides (e.g.,  $Mg_{1-x}Ca_xO$  in Table I). We thus predict that high Mg concentration  $Mg_{1-x}Zn_xO$  alloys will be stable and order in the NaCl (*B1*) structure.

(2) Fourfold-coordinated  $Mg_{1-x}Zn_xO$  alloys have  $\Delta H_{B4} < 0$  for Zn-rich compositions, in contrast with the opposite sign for isostructural *B4* or *B3* alloys,<sup>4</sup> e.g.,  $Cd_{1-x}Zn_xS$ .<sup>6</sup> We thus predict that high Zn concentration  $Mg_{1-x}Zn_xO$  alloys will be stable and order in a fourfold-coordinated structure.

(3) The results (1) and (2) suggest that if coherency with the alloy medium (or epitaxial substrate) can be maintained, such alloys will exhibit *ordering* tendencies at low temperatures, not phase separation like  $Mg_{1-x}Ca_xO$  or  $Cd_{1-x}Zn_xS$ . The remarkable thermodynamic stability  $\Delta H_{\alpha}(Mg_{1-x}Zn_xO) < 0$  results from an unusually small strain energy in the *B1* alloy, due to small lattice mismatch, which is easily overcome by attractive chemical interactions.

(4) To find the stable ordered crystal structures (at  $T = 0$  K) in the *B1*  $Mg_{1-x}Zn_xO$  alloys, one needs to scan, in principle, an astronomic number of possible configurations. We do so by parametrizing the (first-principles calculated) energies of 32 ordered  $Mg_nZn_mO_{n+m}$  structures (not necessarily ground states) in a cluster expansion<sup>7</sup> that readily predicts the energy of *any* *B1* configuration. Searching<sup>8</sup> this

TABLE I. Decomposition of the LDA  $\Delta H_{B1}$  [Eq. (1)] into “volume deformation” ( $\Delta E_{VD}$ ), “charge exchange” ( $\Delta E_{CE}$ ), and “structural relaxation” ( $\Delta E_{SR}$ ) energies, all in meV/cation, for 50–50% alloys modeled via a special quasirandom structure. (See Sec. III.)  $\Delta a/a$  gives the relative lattice constant mismatch between the constituents.

Alloy	$\Delta H_{B1}$	$\Delta E_{VD}$	$\Delta a/a$	$\Delta E_{CE}$	$\Delta E_{SR}$
$Mg_{0.5}Zn_{0.5}O$	−10.8	4.4	1.43	−9.3	−5.9
$Ca_{0.5}Zn_{0.5}O$	55.8	285.6	10.49	−116.7	−113.1
$Ca_{0.5}Mg_{0.5}O$	163.7	327.8	11.88	−57.1	−107.0

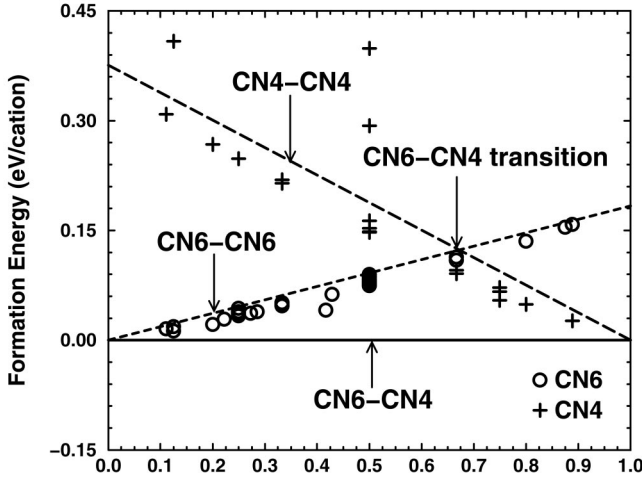


FIG. 1. Calculated total energies of some sixfold-coordinated (CN6) structures (+ symbols) and some of their fourfold-coordinated (CN4) analogs (open circles) [Ref. 11]. For  $x \leq 2/3$  the sixfold structures are lower in energy than their fourfold analogs consistent with the experimental observation (Ref. 9) that a CN6 to CN4 transition occurs at  $x=67\%$ . Three lines connect the end points MgO(CN6)-ZnO(CN6) (solid line), MgO(CN6)-ZnO(CN4) (dashed line), and MgO(CN4)-ZnO(CN4) (long dashed line). The crossover of the CN4-CN4 and CN6-CN6 lines determined by the end-point energies near  $x=67\%$  is also consistent with the observed CN6-CN4 transition.

functional for  $\sim 3 \times 10^6$  possible configurations, we identify  $\text{Mg}_3\text{ZnO}_4$  ( $D0_{22}$ ) and  $\text{Mg}_4\text{Zn}_4\text{O}_8$  as ordered  $B1$ -like ground-state structures.

(5) The formation energy  $E_\alpha$  ( $\text{Mg}_{1-x}\text{Zn}_x\text{O}$ ) changes from being lowest in the sixfold-coordinated structure ( $B1$ ), to being lowest in the fourfold-coordinated ( $B4$ ) structure for Zn concentrations near 67%. This CN6 to CN4 transition has been observed experimentally<sup>9</sup> at  $x_{\text{Zn}}=67\%$ . We see evidence of such a rocksalt-wurtzite transition in Fig. 1, where we compare sixfold-coordinated alloys and their fourfold-coordinated analogs<sup>10</sup> and find that near  $x_{\text{Zn}}=67\%$  the fourfold analogs become more stable than the sixfold structures.

(6) Despite  $\Delta H_{B1} < 0$  and  $\Delta H_{B4} < 0$ , we find that the enthalpy  $\Delta H_{B1,B4}$  taken relative to the *stabllest form* of each end-point constituent (fourfold-coordinated ZnO and sixfold-coordinated MgO),

$$\Delta H_{B1,B4}(\text{Mg}_{1-x}\text{Zn}_x\text{O}) = E_\alpha(\text{Mg}_{1-x}\text{Zn}_x\text{O}) - xE_{B1}(\text{MgO}) - (1-x)E_{B4}(\text{ZnO}), \quad (2)$$

is *positive* for the alloy being in either  $\alpha$  being fourfold- or sixfold-coordinated structures. This means that if coherency with the medium cannot be maintained (so each constituent can adopt its stablest coordination), the alloy will phase separate.

(7) Random alloys of  $\text{Mg}_{1-x}\text{Zn}_x\text{O}$  have a calculated band-gap bowing parameter of  $b=3.1$  eV, in close agreement to recent experimental observations of  $b=3.6 \pm 0.6$  eV.<sup>11</sup> The physical mechanisms responsible for these observations are described in the following section.

Observations (1) and (2) above are shown in Fig. 1, which shows the (first-principles) calculated formation energy<sup>12</sup>  $E_\alpha$  ( $\text{Mg}_n\text{Zn}_m\text{O}_{n+m}$ ) for  $\alpha=\text{CN4}$  ordered structures and for  $\alpha=\text{CN6}$  ordered structures. For the end-point compounds, we find that MgO is stable in the CN6 ( $B1$ ) form. The CN4 ( $B4$ ) form of ZnO is 206 meV/cation higher than CN6 ( $B1$ ). The energies of the CN6- $\text{Mg}_{1-x}\text{Zn}_x\text{O}$  alloys are below the (MgO, CN6)-(ZnO, CN6) tie line for  $x_{\text{Zn}} \leq 67\%$ , and the energy of the CN4- $\text{Mg}_{1-x}\text{Zn}_x\text{O}$  alloys are below the (MgO, CN4)-(ZnO, CN4) tie line for  $x_{\text{Zn}} \geq 67\%$ . Thus, CN6 ( $B1$ ) alloys are stable for  $x_{\text{Zn}} < 67\%$  whereas CN4 alloys are stable for  $x_{\text{Zn}} \geq 67\%$ , consistent with the extended solid solubility observed in this system.<sup>5</sup>

### III. PHYSICAL ORIGINS OF HETEROSTRUCTURAL STABILITY

To clarify the origin of this unexpected stability, we decomposed  $\Delta H_{B1}$  into three physically recognizable components.<sup>16</sup>

(i) the “volume deformation” component  $\Delta E_{\text{VD}}$  due to the dilation  $B1$ -MgO and compression of  $B1$ -ZnO from their equilibrium lattice parameters (4.16 Å and 4.22 Å, respectively) to the common (Vegard-like) lattice constant of the alloy.

(ii) The “charge exchange” energy  $\Delta E_{\text{CE}}$  released when MgO and ZnO, already prepared at common lattice constant, combine to give  $\text{Mg}_{0.5}\text{Zn}_{0.5}\text{O}$  in a random arrangement, modeled via the “quasirandom structures” concept.<sup>17</sup> At this constant-volume reaction all cell-internal degrees of freedom of the alloy are held fixed at their ideal positions.

(iii) The “structural relaxation” energy  $\Delta E_{\text{SR}}$  released when the cell-internal degrees of freedom of the random alloy are relaxed. Thus,  $\Delta H = \Delta E_{\text{VD}} + \Delta E_{\text{CE}} + \Delta E_{\text{SR}}$ .

Table I shows that in  $B1$ - $\text{Ca}_{0.5}\text{Zn}_{0.5}\text{O}$  and  $B1$ - $\text{Ca}_{0.5}\text{Mg}_{0.5}\text{O}$ , the large size mismatch ( $\Delta a/a$ ) between the constituents leads to a very large and positive  $\Delta E_{\text{VD}}$  that overwhelms  $\Delta E_{\text{CE}} + \Delta E_{\text{SR}}$ . On the other hand, in  $B1$ - $\text{Mg}_{0.5}\text{Zn}_{0.5}\text{O}$  the volume deformation energy is very small (owing to the small lattice mismatch), and the negative charge-exchange and the structural-relaxation energies prevail, leading to  $\Delta H_{B1} < 0$ . We have carefully tested that this basic result is not changed when we use a linearized augmented plane wave method (WIEN97) instead of pseudopotentials, or when we replace the local-density approximation (LDA) by a generalized gradient approximation. Results of these tests are shown in Table II.

Stolbov and Cohen<sup>18</sup> have recently calculated the mixing enthalpy of CaO-MgO assuming the spherical muffin-tin approximation (rather than full potential), and neglecting cell internal atomic relaxation, finding for the 50–50% alloy  $\Delta H \approx 300$  meV. This is much higher than our result for the same alloy (163.7 meV, Table I). The difference can be mostly attributed to the neglect of cell internal relaxation ( $\Delta E_{\text{SR}} \approx -110$  meV term in Table I).

### IV. MODELING THE MgO-ZnO ALLOY

#### A. The cluster expansion

Having established that the CN6, Mg-rich  $\text{Mg}_{1-x}\text{Zn}_x\text{O}$  alloy will order, the next question is what ordered structures

TABLE II. Cubic ( $a$ ) and tetragonal ratio ( $c/a$ ) of lattice constants and formation energies of selected  $B1$  structures using pseudopotential (PP) method within LDA and GGA approximation and LDA-LAPW method. The units for the lattice constants and formation energies are in angstroms and meV/cation, respectively.

Alloy	PP	PP	LAPW	PP	PP	LAPW
	LDA	GGA	LDA	LDA	GGA	LDA
		$a, c/a$			$\Delta H$	
MgO	4.16, 1	4.24, 1	4.17, 1			
ZnO	4.22, 1	4.33, 1	4.20, 1			
$L1_2$	4.18, 1	4.27, 1	4.18, 1	-11.0	-10.4	-13.3
$DO_{22}$	4.17, 1.001	4.27, 1.002	4.17, 1.001	-12.7	-12.0	-14.9
$L1_0$	4.19, 0.998	4.29, 0.998	4.19, 0.998	-15.1	-13.2	-17.3

are the most stable. To answer this we have parametrized 32  $B1$  total-energy calculations of  $Mg_mZn_nO_{m+n}$  structures (shown as open squares in Fig. 2) into a cluster expansion. Within the cluster-expansion method<sup>7</sup> one selects an underlying parent lattice (e.g., fcc) and defines a configuration  $\sigma$  by specifying the occupations of each of the lattice sites by an  $A$  or a  $B$  atom (spin index  $S_i = -1$  and  $+1$ , respectively). The excess energy (with respect to equivalent amounts of solid  $A$  and  $B$ ) of any spin configuration  $\sigma$ , at its locally atomically-relaxed minimum-energy state is then expanded as

$$\Delta H_{CE}(\sigma) = \sum_{\mathbf{k}} J_{\text{pair}}(\mathbf{k}) |S(\mathbf{k}, \sigma)|^2 + \sum_f D_f J_f \bar{\Pi}_f(\sigma) + \sum_{\mathbf{k}} \frac{\Delta E_{CS}(x, \hat{k})}{4x(1-x)} |S(\mathbf{k}, \sigma)|^2 F(\mathbf{k}). \quad (3)$$

The first summation includes all pair figures corresponding to pair interactions with arbitrary separation.  $J_{\text{pair}}(\mathbf{k})$  is the Fourier transform of the pair interaction energies and  $S(\mathbf{k}, \sigma)$

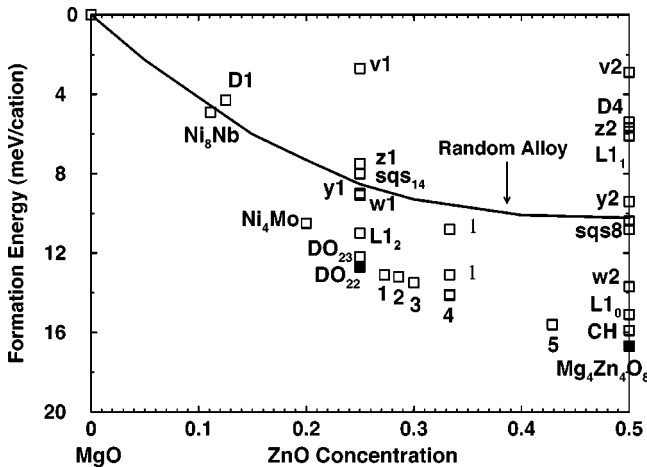


FIG. 2. LDA-formation energies and CE predicted energies. LDA calculated formation energies [Eq. (1)] are shown as open squares. The ground states predicted by the cluster expansion are indicated as solid squares. The energy of the random alloy is given by the solid line. The numbers 1, 2, 3, 4, and 5, refer to the structures  $Mg_3Zn_3O_{11}$ ,  $Mg_5Zn_2O_7$ ,  $Mg_7Zn_3O_{10}$ ,  $Mg_4Zn_2O_6$ , and  $Mg_4Zn_3O_7$ , respectively.

the structure factor of configuration  $\sigma$ . The second sum includes only nonpair figures. Here  $J_f$  is the real-space effective many-body interactions of figure  $f$ ,  $D_f$  stands for the number of equivalent clusters per lattice site, and  $\bar{\Pi}_f(\sigma)$  are spin products. The third summation represents atomic size-mismatch effects and involves the “constituent strain” energy  $\Delta E_{CS}(x, \hat{k})$  necessary to maintain coherency between  $A$  and  $B$  along an interface with orientation  $\hat{k}$ , and  $F(\mathbf{k})$  is the attenuation function for short wavelengths. This third term gives rise to a long-range interaction in real space and includes the necessary nonanalytic,  $k \rightarrow 0$ , behavior.<sup>7</sup>

The terms  $\Delta E_{CS}^{\text{eq}}(x, \hat{k})$  and  $\Delta H(\sigma)$  in Eq. (3) are determined from first-principles total-energy calculations.  $\Delta E_{CS}^{\text{eq}}(x, \hat{k})$  is obtained from a set of calculations on biaxially strained  $A$  and  $B$  solids. We determine  $\{J_{\text{pair}}(\mathbf{k})\}$  and  $\{J_f\}$  by fitting  $\Delta H_{CE}(\sigma_{\text{ord}})$  to a set  $\{\sigma_{\text{ord}}\}$  of LDA calculated formation energies  $\Delta H_{\text{LDA}}(\sigma_{\text{ord}})$  of ordered (not necessarily ground states)  $A_pB_q$  compounds. For each structure, we relax both the cell-external lattice vectors and the atomic cell-internal degrees of freedom to obtain minimum energies. The interactions in Eq. (3) ( $J_f$  and  $J_{\text{pair}}$ ) were chosen to minimize both the fitting errors and the prediction errors. This is done by eliminating from the fit several of the ordered structures  $\{\sigma_{\text{ord}}\}$  and choosing the interactions that result in an accurate fit to the structures retained *as well as* accurate predictions for the eliminated structures. The process is repeated using different sets of eliminated structures to ensure a set of interactions that work well generally. We find that only 20 pair interactions and three many-body interactions, along with the (infinitely ranged) strain pair interactions, are needed to obtain a fit error of 0.26 meV/cation and a prediction error of 1.67 meV/cation.

## B. Finding the ground states

Using the function  $\Delta H_{CE}(\sigma)$ , we have searched the energy of all supercells with a total of  $n + m = 20$  cations (more than  $3 \times 10^6$  structures in total). Figure 3 shows the results of this ground-state search. The “breaking points” correspond to the structures that are both the lowest of all possible structures at a given composition *and* stable with respect to phase separation into competing structures at other compositions. We determined that the LDA-calculated energy of the ground-state structures agrees with the cluster-expansion pre-

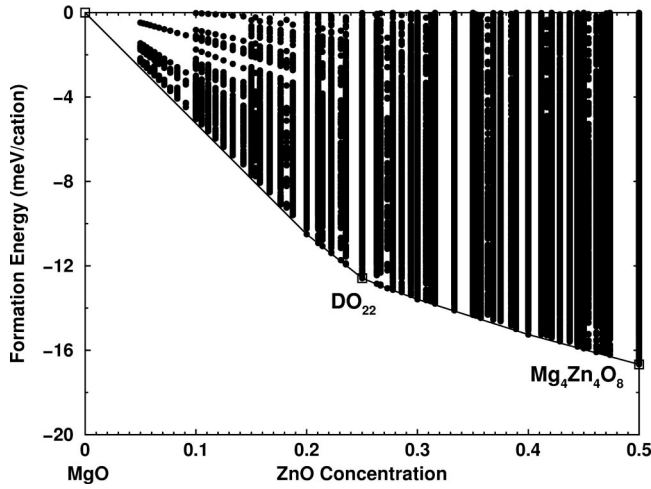


FIG. 3. Ground-state search for  $B1\text{-Mg}_{1-x}\text{Zn}_x\text{O}$  alloys. The stable ground states are denoted by open squares.

dictions within 0.3 meV/atom. Although several “breaking points” exist, the energetically “deepest” structures occur at  $x=0.25$  and  $x=0.5$ . For  $x=0.25$ , the ground state is a  $DO_{22}$ -type structure with lattice constants  $a=4.174$  Å and  $c=4.179$  Å. For  $x=0.50$ , the ground state is an orthorhombic structure with lattice constants  $a=4.189$  Å,  $b=4.187$  Å, and  $c=8.900$  Å. The atomic positions and lattice vectors of predicted ground states are shown in Table III. The common structural motif for these ground-state structures is that they are (201) superstructures. It is known that (201) superstructures have low Madelung energies<sup>7</sup> and our calculations show that the constituent strain energy along the (201) direction is softer with respect to the other principal directions.

### C. Thermodynamic modeling

Figure 2 shows the energy of the random  $B1$  solid solutions (solid line), obtained by performing high-temperature (40000 K) Monte Carlo simulations with Hamiltonian,  $E_{CE}(\sigma)$ . The open symbols denote the energies of ordered structures, used as input to the cluster expansion, whereas the energies of the ground-state structures are denoted by solid squares. We see that the energy difference between the stable ordered ground-state structures and the random alloy of the same composition (e.g.,  $x=0.5$ ) is rather small ( $-6.5$  meV/

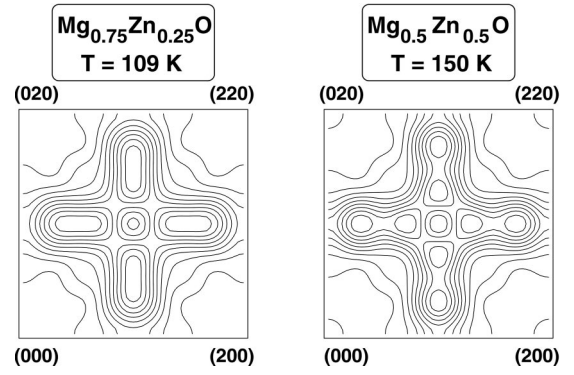


FIG. 4. Short-range-order patterns of the predicted ground states at a temperature  $T=1.9 T_c$ . Numbers at the corners of the plots refer to locations in reciprocal space, i.e., vertices of the Brillouin zone.

cation), so the order-disorder transition temperature will be well below conventional growth temperatures (Monte Carlo simulations give  $T_c=79$  K). Nevertheless, ordering tendencies could be monitored even in the disordered alloy by observing its short-range-order (SRO) patterns. Figure 4 shows our calculated SRO obtained from Monte Carlo simulation of the cluster-expanded energy at finite temperatures. Clear ordering signatures (peaks away from the Brillouin-zone centers) are predicted.

Figure 1 shows that the  $\text{Mg}_{1-x}\text{Zn}_x\text{O}$  alloy has a lower absolute total energy in the sixfold-coordinated structure than in fourfold-coordinated structure up to  $x_{\text{Zn}} \approx 0.67\%$ , but that beyond this region the fourfold-coordinated structure is more stable. This CN6 to CN4 transition has also been calculated by Kim *et al.*<sup>19</sup> and observed<sup>9</sup> by Ohtomo *et al.* Figure 1 also demonstrates that both CN4 and CN6 ordered alloys have higher energies than the stablest forms of the constituents. This indicates that once coherency is lost, and a coexistence of  $B1\text{-MgO}$  with  $B4\text{-ZnO}$  precipitates is possible, the alloy will phase separate. Indeed, such tendencies were seen experimentally.<sup>20</sup>

### V. CONCLUSIONS

We conclude that the  $B1\text{-Mg}_{1-x}\text{Zn}_x\text{O}$  alloys have  $\Delta H_{B1} < 0$  due to small elastic strains and favorable chemical energy, forming low-temperature ordered  $\text{Mg}_3\text{ZnO}_4$  and  $\text{Mg}_4\text{Zn}_4\text{O}_8$  structures and distinct short-range-order patterns

TABLE III. Predicted ground states by the CE for  $\text{Mg}_{1-x}\text{Zn}_x\text{O}$  system. Atomic positions of oxygen atoms can be found by shifting the atomic positions of Mg and Zn by (0.5, 0.5, 0.5).

Structure	Lattice vectors	Atomic positions
$\text{Mg}_3\text{ZnO}_4$ ( $DO_{22}$ )	0 1 0 $-\frac{1}{2} -\frac{1}{2} 1$ 1 0 0	Mg (0, 0, 0), Mg (-0.5, 0, 0.5) Mg (-0.5, 0.5, 0), Zn (0.5, 0, -0.5)
$\text{Mg}_4\text{Zn}_4\text{O}_8$	1 0 0 0 1 0 $\frac{1}{2} \frac{1}{2} 2$	Mg (0.5, 0.5, 0), Mg (1, 0.5, 0.5) Mg (0.5, 0.5, 1), Mg (1, 0.5, 1.5) Zn (0, 0, 0), Zn (0.5, 1, 0.5) Zn (1, 1, 1), Zn (0.5, 1, 1.5)

at high temperatures. The random alloy has an LDA band gap of 2.49 eV at  $x=0.5$  (using a special quasirandom structure<sup>17</sup>), and hence a bowing coefficient  $b_{\text{bowing}} = 3.10$  eV, where  $E_g(x) = (1-x)E_{\text{MgO}} + xE_{\text{ZnO}} - x(1-x)b_{\text{bowing}}$ . This value of the bowing coefficient is in good agreement with the value of  $3.6 \pm 0.6$  eV measured recently by Schmidt *et al.*<sup>10</sup> The ordered structure at  $x=0.5$  has a lower band gap than the random alloy by 0.39 eV. There is a CN6 to CN4 transition for  $x_{\text{Zn}} > 0.67\%$ , whereas the coher-

ent alloy is *B1* stable below this composition. If MgO and ZnO can (incoherently) adopt their own crystal structures (*B1* and *B4*, respectively), the alloy is predicted to phase separate.

#### ACKNOWLEDGMENT

This work was supported by the U.S. Department of Energy, SC-BES-OER Grant No. DE-AC36-98-GO10337.

- 
- <sup>1</sup>E. Parthe, *Crystal Chemistry of Tetrahedral Structures* (Gordon and Breach, New York, 1964).
- <sup>2</sup>P.K. Davies and A. Navrotsky, *J. Solid State Chem.* **46**, 1 (1983).
- <sup>3</sup>*Phase Diagrams for Ceramists*, edited by E. M. Levin, C. R. Robbins, and H. F. McMurdies (American Ceramic Society, Columbus, OH, 1969); see also E.R. Segnit and A.E. Holland, *J. Am. Ceram. Soc.* **48**, 412 (1965).
- <sup>4</sup>S.H. Wei and A. Zunger, *Phys. Rev. B* **37**, 8958 (1988); **43**, 1662 (1991); *J. Vac. Sci. Technol. A* **6**, 2597 (1988); *J. Cryst. Growth* **86**, 1 (1988).
- <sup>5</sup>A. Ohtomo, M. Kawasaki, Y. Sakurai, Y. Yoshida, H. Koinuma, P. Yu, Z.K. Tang, G.K.L. Wong, and Y. Segawa, *Mat. Sci. Eng.* **56**, 263 (1998); J.H. Kang, Y.R. Park, and K.J. Kim, *Solid State Commun.* **115**, 127 (2000); A.K. Sharma, J. Narayan, J.F. Muth, C.W. Teng, C. Jin, A. Kvit, R.M. Kolbas, and O.W. Holland, *Appl. Phys. Lett.* **75**, 3327 (1999); Y. Jin, B. Zhang, S. Yang, Y. Wang, J. Cjen, H. Zhang, C. Huang, C. Cao, H. Cao, and R.P.H. Chang, *Solid State Commun.* **119**, 409 (2001).
- <sup>6</sup>S.H. Wei, S.B. Zhang, and A. Zunger, *J. Appl. Phys.* **87**, 1304 (2000).
- <sup>7</sup>A. Zunger, in *Statics and Dynamics of Alloy Phase Transformation*, edited by P. E. A. Turchi and A. Gonis (Plenum, New York, 1994); D.B. Laks, S. Froyen, L.G. Ferreira, and A. Zunger, *Phys. Rev. B* **46**, 12 587 (1992).
- <sup>8</sup>L.G. Ferreira, S.-H. Wei, and A. Zunger, *Int. J. Supercomput. Appl.* **5**, 34 (1991).
- <sup>9</sup>A. Ohtomo, M. Kawasaki, T. Koida, K. Masubuchi, H. Koinuma, Y. Sakurai, Y. Yoshida, T. Yasuda, and Y. Segawa, *Appl. Phys. Lett.* **72**, 2466 (1998); T. Minemoto, T. Negami, S. Nishiwaki, H. Takakura, and Y. Hamakawa, *Thin Solid Films* **372**, 173 (2000).
- <sup>10</sup>The positions of the magnesium and zinc atoms in the sixfold structures and their fourfold analogs are the same, that is, the occupations of the metal fcc sublattice (centered at  $[0,0,0]$ ) are identical. In the fourfold analogs, the oxygen site is shifted to  $(1/4, 1/4, 1/4)a_0$  from  $(1/2, 1/2, 1/2)a_0$ . Because a structure and its analog are identical except for oxygen coordination, their energy difference reveals the effect of oxygen coordination only and is not affected by differences in alloy configuration.
- <sup>11</sup>R. Schmidt, C. Bundesmann, N. Ashkenov, B. Rheinländer, M. Schubert, M. Lorenz, E.M. Kaidashev, D. Spemann, T. Butz, J. Lenzer, M. Grundmann, *Proceedings of the 26th International Conference on the Physics of Semiconductors, Edinburgh (ICPS-26)*, Institute of Physics Series Vol. 171, edited by A.R. Long and J.H. Davies (Institute of Physics, Bristol, 2002), p. 11.
- <sup>12</sup>We use the local-density approximation (LDA) within a plane-wave total-energy formalism (Ref. 13), using ultrasoft pseudopotentials (Ref. 14) as implemented in the VASP package (Ref. 15). We use a highly converged basis set and an equivalent  $k$ -point mesh to assure precision of 0.1 meV/cation for the calculated formation energies. For  $AB$  and  $A_2B$  ( $AB_2$ ) stoichiometries we choose  $8 \times 8 \times 8$  and  $9 \times 9 \times 9$   $\mathbf{k}$  meshes, respectively.
- <sup>13</sup>J. Ihm, A. Zunger, and L. Cohen, *J. Phys. C* **12**, 4409 (1979).
- <sup>14</sup>D. Vanderbilt, *Phys. Rev. B* **41**, 7892 (1990).
- <sup>15</sup>G. Kresse and J. Furthmüller, *Phys. Rev. B* **54**, 11 169 (1996); *Comput. Mater. Sci.* **6**, 15 (1996).
- <sup>16</sup>J.E. Bernard and A. Zunger, *Phys. Rev. B* **36**, 3199 (1987); S.H. Wei and A. Zunger, *Phys. Rev. Lett.* **76**, 664 (1996).
- <sup>17</sup>A. Zunger, S.H. Wei, L.G. Ferreira, and J.E. Bernard, *Phys. Rev. Lett.* **65**, 353 (1990).
- <sup>18</sup>S.V. Stolbov and R.E. Cohen, *Phys. Rev. B* **65**, 092203 (2002).
- <sup>19</sup>Y.S. Kim, E.C. Lee, and K.J. Chang, *J. Korean Phys. Soc.* **39**, S92 (2001).
- <sup>20</sup>S.A. Chudinova and O.N. Shvyrin, *Sov. Phys. Solid State* **14**, 1297 (1972).